Journal of Magnetism and Magnetic Materials 326 (2013) 116–122

Contents lists available at SciVerse ScienceDirect

Journal of Magnetism and Magnetic Materials

journal homepage: www.elsevier.com/locate/jmmm

A multiscale model for thin film AMR sensors

András Bartók [a], Laurent Daniel [a,b,*], Adel Razek [a]

[a] Laboratoire de Génie Électrique de Paris, CNRS (UMR 8507)/SUPELEC/UPMC/Univ Paris-Sud, 11 rue Joliot Curie, 91192 Gif sur Yvette, France
[b] Materials Science Centre, University of Manchester, M1 7HS Manchester, UK

ARTICLE INFO

Article history:
Received 17 July 2012
Available online 5 September 2012

Keywords:
AMR sensor
Micro–macro modeling
Magnetoresistance
Magnetic field sensing

ABSTRACT

AMR sensors are among the most widely deployed magnetic field sensors. In contrast to other technologies it has a simple structure and a low production cost. In this paper a multiscale modeling strategy is proposed to describe the performance of these sensors taking their specific features into account. The prediction of the behavior of a typical AMR thin film sensor has been studied and the results are compared to experimental measurements from the literature. The proposed micro–macro model offers an opportunity to investigate optimal material composition, crystallographic texture, film thickness or bias field level for specific applications.

0. Introduction

Anisotropic Magnetoresistance (AMR) effect in ferromagnetic materials is the dependence of the electrical resistivity on the angle between the direction of the electrical current and the magnetization [1]. This effect is the basis for a wide range of magnetic field sensors. These sensors are mostly made of ferromagnetic thin films. The application of a magnetic field changes the magnetization of the film, and the corresponding change in resistivity is measured through an electronic circuit. These devices can be used as magnetic field detectors according to the *all-or-nothing* operation method. They can then be part of displacement, position or rotation speed sensors in electro-mechanical machines [2,3]. AMR devices can also be used for the quantitative measurement of magnetic field. This type of AMR sensors is used in electronic compasses (measurement of Earth's magnetic field) [4] and for non-contact detection of electrical currents (by measuring the magnetic field created around the conductor) [5].

Several technologies can be used to ensure an optimal performance for these sensors [6–9], but this performance is always related to the intricate relationship between the microstructure and the macroscopic response of the sensor. In the case of ferromagnetic polycrystalline materials, the microstructure scale is twofold. The material is divided into magnetic domains with different magnetizations, and it is also divided into grains with different crystallographic orientations.

From the modeling point of view, a large part of phenomenological models for the AMR effect are based on the hypothesis that the material is at magnetic saturation so that it can be described as a one-domain particle [10–14]. This is however a strong simplification due to the complex magnetic domain structure of ferromagnetic materials. Some authors proposed micromagnetic calculations to describe this evolving domain structure in thin film AMR sensors [15,16]. But these approaches usually lead to dissuasive computation time so that strong simplifying assumptions are needed when describing real systems. An alternative is the use of a micro–macro approach that incorporates a statistical view of the microstructure to define the effective properties of ferromagnetic materials [17,18]. Such an approach has been recently applied to the AMR effect for bulk ferromagnetic polycrystals [19].

In this paper this micro–macro approach is extended to describe the properties of thin film AMR sensors. A demagnetizing surface effect is introduced in order to account for the small thickness of the material, and the specific crystallographic texture of AMR sensors is introduced. This model allows us to reproduce the features of AMR magnetic field sensors under typical operating conditions.

The paper is divided into four parts. In the first part the operation principle and the fabrication technology of thin film permalloy AMR sensors are briefly presented. In the second part the modeling strategy is detailed. This approach is then applied in the third part to the prediction of the behavior of a typical AMR sensor. The results are compared to the experimental results obtained from the literature. The last part is a discussion on the role of the bias field and film thickness in the optimization of the sensors performance.

1. Thin film AMR sensors

An AMR sensor has two main parts, a magnetoresistive sensor element and a comparator circuit prepared on one chip. The

* Corresponding author at: Laboratoire de Génie Électrique de Paris, CNRS (UMR 8507)/SUPELEC/UPMC/Univ Paris-Sud, 11 rue Joliot Curie, 91192 Gif sur Yvette, France. Tel.: +33 1 69 85 16 39; fax: +33 1 69 41 83 18.
E-mail address: laurent.daniel@lgep.supelec.fr (L. Daniel).

0304-8853/$ - see front matter © 2012 Elsevier B.V. All rights reserved.
http://dx.doi.org/10.1016/j.jmmm.2012.08.020

sensor elements are typically made of highly textured thin permalloy films deposited on a silicon wafer and patterned as a resistive strip [6]. Thanks to the thin film structure the magnetization remains mostly in the film plane so that the film behavior is insensitive to the perpendicular component of the external field.

As the electrical resistivity depends on the angle between the direction of the electrical current and the magnetization, a close-saturation magnetization state can ensure the ideal sensing properties. The permalloy film element (xy plane) is deposited in a strong magnetic field that sets the preferred orientation (macroscopic easy axis, x). It results in a strong orientation of crystallographic easy magnetic axes along the x direction. In the case of the absence of external magnetic field the macroscopic magnetization vector is set parallel to the length of the resistor and can be set to point in either direction, left or right in the film. The component of the external magnetic field measured by the sensor will then be the y component (Fig. 1).

As a first step before the real field measurement, an external magnetic field can be used to align the magnetic domains in the preferred direction (reset procedure). During the measurement, a bias magnetic field (created by additional hard magnets or coils) is applied in direction x so that the magnetization aligns with the x axis. The sensor is then unidirectional, it is only sensitive to the y component of the external field. This y component tends to rotate the magnetization in the film plane which results in a detectable change in the electrical resistivity of the sensor element. Nevertheless, the x component of the external field must remain low enough to avoid a change in the sign of the original magnetization (*flipping-effect*). The bias field has an effect on the measurement range and the sensitivity of the sensor, and its value must be carefully set depending on the application.

The first generation of AMR thin film sensors was used in the read head of hard disk drives. The sensor elements had *single-path* structure as it is presented in Fig. 2. Here the electrical current (dark lines) flows in the easy direction (x) of the film. A perturbation field in the z direction (diffused magnetic field of a magnetic bit on the hard disk for example) changes the resistivity. This device has been used in the *all-or-nothing* operation method.

If a quantitative measurement of the magnetic field is necessary, then a linear response of the sensor is preferred. An electrical current oriented 45° from the x axis can ensure this linearity. These sensors use a layout technique that places low-resistance shorting bars (so called *barber-pole*) oriented 45° from the x axis, as presented in Fig. 3. The current, following the shortest path, flows from one bar to the next at a 45° angle.

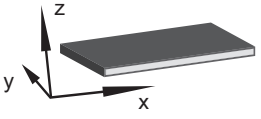

Fig. 1. Magnetic field sensor. x: Macroscopic easy magnetization axis and y: measurement direction.

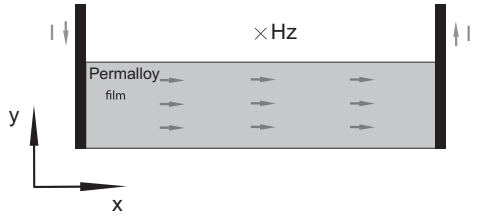

Fig. 2. *Single-path* sensor.

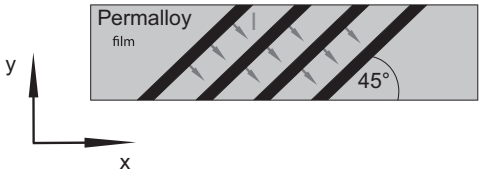

Fig. 3. *Barber-pole* sensor element.

In the magnetoresistive sensor elements four of these resistors are connected in a Wheatstone bridge to compensate the temperature-dependence effects.

The comparator circuit adds a linear amplification to the sensor element's signal. So finally the change in the output voltage of the sensor is proportional to the change in resistivity of the AMR thin film. If the sensor is used in the linear range, then this change in resistivity is itself proportional to the y component of the external magnetic field.

The object of the next part is the detail of a multiscale approach to describe these types of sensor configuration.

2. A multiscale approach

When dealing with heterogeneous microstructures and complex physical mechanisms, multiscale approaches can be an efficient tool for the prediction of macroscopic behavior. It is based on the principle that a relevant description of the physical mechanisms can be written at the scale of the typical heterogeneities of the material—here the magnetic domains. This approach supposes to be able to estimate the local loading (stress, magnetic field, electric current) as a function of the applied loading. This is made through scale transition rules, depending on the microstructure of the material. In the case of thin film magnetoresistive sensors, two important parameters need to be considered in addition. The first one is the sharp crystallographic texture of these thin films that has a strong impact on the overall behavior. The second one is the small thickness of the films that induces strong demagnetizing effects and affects the magnetic behavior.

The model proposed in this paper is detailed hereafter. The description is divided into three parts. The localization rules to define the local loading as a function of the external loading are first presented. The local constitutive law is then detailed and the homogenization step to define the macroscopic response is finally explained. The model is an extension of a previously published model for bulk magnetoresistive materials [19]. The main change is the introduction of a demagnetizing surface term to describe thin film behavior and the introduction of a sharp texture representative for standard thin film AMR sensors.

2.1. Localization rules

The macroscopic loading is given by the macroscopic current $\bar{\mathbf{I}}$, the applied stress $\bar{\boldsymbol{\sigma}}$ and the applied magnetic field $\bar{\mathbf{H}}$. The aim of the localization step is to define the local loading, at the scale of the typical heterogeneities, as a function of this macroscopic loading. The scale transition rules are given in [19] and extensively discussed in [17]. They are briefly presented hereafter. Two distinct scales have to be considered: the scale of the magnetic heterogeneities (magnetic domains, index α) and the scale of the mechanical heterogeneities (grains in the polycrystal, index g).

Due to the weak electrical heterogeneity, the current $\mathbf{i}$ is assumed to be uniform

$$\mathbf{i}_\alpha = \mathbf{i}_g = \bar{\mathbf{I}} \tag{1}$$

The stress $\boldsymbol{\sigma}_\alpha$ at the magnetic domain scale is not needed in the following. The stress $\boldsymbol{\sigma}_g$ at the grain scale is defined using localization operators

$$\boldsymbol{\sigma}_g = \mathcal{B}_\sigma : \overline{\boldsymbol{\sigma}} + \mathcal{L}^{\text{inc}} : (\overline{\boldsymbol{\varepsilon}^\mu} - \boldsymbol{\varepsilon}_g^\mu) \tag{2}$$

$\overline{\boldsymbol{\varepsilon}^\mu}$ and $\boldsymbol{\varepsilon}_g^\mu$ are the magnetostriction strain respectively at the macroscopic and grain scale. $\mathcal{B}_\sigma$ denotes the so-called stress concentration tensor and $\mathcal{L}^{\text{inc}}$ is a tensor accounting for elastic incompatibilities due to magnetostriction. Tensors $\mathcal{B}_\sigma$ and $\mathcal{L}^{\text{inc}}$ highly depend on the orientation of the considered grain, so that crystallographic texture effects can be accounted for through (2). Since the magnetostriction strain is not initially known an iterative process is needed (see Section 2.4). The reader is referred to the previous publications [17,19] for the calculation procedures of $\mathcal{B}_\sigma$ and $\mathcal{L}^{\text{inc}}$.

The magnetic field is supposed to be uniform at the grain scale ($\mathbf{H}_\alpha = \mathbf{H}_g$). Although inaccurate, this assumption allows us to define the behavior of a grain on average. The magnetic field $\mathbf{H}_g$ at the grain scale is defined through the following localization equation [17,19]:

$$\mathbf{H}_g = \overline{\mathbf{H}} + \frac{1}{3+2\chi^m}(\overline{\mathbf{M}} - \mathbf{M}_g) \tag{3}$$

$\overline{\mathbf{M}}$ and $\mathbf{M}_g$ are the magnetization, respectively, at the macroscopic and grain scale and χ^m is the effective magnetic susceptibility of the material. Again, this equation requires an iterative process to be solved.

Once the local loading is defined, a local constitutive law has to be applied.

2.2. Local constitutive law

The local constitutive law is written at the scale of a single crystal or a grain in a polycrystal. A grain (index g) is seen as a collection of magnetic domains α with uniform magnetization $\mathbf{M}_\alpha$ oriented along direction $\boldsymbol{\alpha} = {}^t[\alpha_1\ \alpha_2\ \alpha_3]$ (that can be any unit vector). The norm of $\mathbf{M}_\alpha$ is M_s the saturation magnetization of the material. Inside a magnetic domain α, the magnetostriction strain $\boldsymbol{\varepsilon}_\alpha^\mu$ is also uniform. In the case of cubic crystallographic symmetry, the magnetostriction strain tensor can be written as

$$\boldsymbol{\varepsilon}_\alpha^\mu = \frac{3}{2}\begin{pmatrix} \lambda_{100}(\alpha_1^2 - \frac{1}{3}) & \lambda_{111}\alpha_1\alpha_2 & \lambda_{111}\alpha_1\alpha_3 \\ \lambda_{111}\alpha_1\alpha_2 & \lambda_{100}(\alpha_2^2 - \frac{1}{3}) & \lambda_{111}\alpha_2\alpha_3 \\ \lambda_{111}\alpha_1\alpha_3 & \lambda_{111}\alpha_2\alpha_3 & \lambda_{100}(\alpha_3^2 - \frac{1}{3}) \end{pmatrix} \tag{4}$$

where λ_{100} and λ_{111} are the magnetostrictive constants of the single crystal.

We call domain family α the set of magnetic domains with magnetization $\mathbf{M}_\alpha$ along direction $\boldsymbol{\alpha}$ in a grain. The free energy of a domain family α can be divided into four contributions (5)

$$W_\alpha = W_\alpha^K + W_\alpha^H + W_\alpha^\sigma + W_\alpha^S \tag{5}$$

W_α^K is the magnetocrystalline anisotropy energy. In the case of a cubic crystallographic symmetry it is expressed as a function of the magneto-crystalline anisotropy constants K_1 and K_2

$$W_\alpha^K = K_1(\alpha_1^2\alpha_2^2 + \alpha_2^2\alpha_3^2 + \alpha_3^2\alpha_1^2) + K_2(\alpha_1^2\alpha_2^2\alpha_3^2) \tag{6}$$

This paper has been focused on polycrystalline materials, this is why magnetocrystalline energy is introduced. However, other type of anisotropy could also be considered, such as uniaxial anisotropy for amorphous or nanocrystalline AMR thin films.

W_α^H is the magnetostatic energy, tending to align the magnetization with the local magnetic field $\mathbf{H}_\alpha$

$$W_\alpha^H = -\mu_0 \mathbf{M}_\alpha \cdot \mathbf{H}_\alpha \tag{7}$$

W_α^σ is the magnetoelastic energy accounting for the effect of stress on the magnetic behavior, introducing the average stress within the grain $\boldsymbol{\sigma}_g$

$$W_\alpha^\sigma = -\boldsymbol{\sigma}_g : \boldsymbol{\varepsilon}_\alpha^\mu \tag{8}$$

Compared to the initial model presented in [19], an additional contribution is introduced. W_α^S is the surface energy, accounting for the strong demagnetizing effects due to the small thickness of the films. Such a demagnetizing term was proposed in [20] to describe the magneto-elastic behavior of Iron–Silicon Grain Oriented sheets. It can be written as

$$W_\alpha^S = N_S(\boldsymbol{\alpha} \cdot \mathbf{z})^2 \tag{9}$$

$\mathbf{z}$ is the direction normal to the film and N_S is the demagnetizing field energy.

Concerning the resistivity ρ_α of a domain family α, it can be defined according to the Döring model [10,21]. For instance, for a cubic crystal with negative anisotropy constant, it can be written as

$$\begin{aligned}\rho_\alpha = \rho_0 \Bigg[1 &+ k_1\left(\alpha_1^2\beta_1^2 + \alpha_2^2\beta_2^2 + \alpha_3^2\beta_3^2 - \frac{1}{3}\right) \\ &+ 2k_2(\alpha_1\alpha_2\beta_1\beta_2 + \alpha_2\alpha_3\beta_2\beta_3 + \alpha_3\alpha_1\beta_3\beta_1) + k_3\left(s - \frac{1}{3}\right) \\ &+ k_4\left(\alpha_1^4\beta_1^2 + \alpha_2^4\beta_2^2 + \alpha_3^4\beta_3^2 + \frac{2s}{3} - \frac{1}{3}\right) \\ &+ 2k_5(\alpha_1\alpha_2\beta_1\beta_2\alpha_3^2 + \alpha_2\alpha_3\beta_2\beta_3\alpha_1^2 + \alpha_3\alpha_1\beta_3\beta_1\alpha_2^2)\Bigg]\end{aligned} \tag{10}$$

where $\boldsymbol{\beta} = {}^t[\beta_1\ \beta_2\ \beta_3]$ is the current direction (unit vector), $s = \alpha_1^2\alpha_2^2 + \alpha_2^2\alpha_3^2 + \alpha_3^2\alpha_1^2$, ρ_0 is the resistivity of the material in the demagnetized state and k_1, k_2, k_3, k_4, k_5 are material constants.

After this description of the local state for a domain family α, we introduce a state variable f_α representing the volume fraction of domains with magnetization along $\boldsymbol{\alpha}$ in a grain g. This volume fraction f_α is obtained through an explicit expression [22]:

$$f_\alpha = \frac{\exp(-A_S \cdot W_\alpha)}{\int_\alpha \exp(-A_S \cdot W_\alpha)\, d\alpha} \tag{11}$$

A_S is an adjustment parameter related to the initial slope of the anhysteretic magnetization curve [17]. The domain structure is then described in a statistical way.

Once the constitutive law has been applied, a set of volume fraction f_α is associated with a set of direction $\boldsymbol{\alpha}$ regularly distributed in space. An averaging operation then allows us to estimate the macroscopic response: it is the homogenization step.

2.3. Homogenization step

The magnetostriction strain and magnetization within a single crystal (or grain) are defined by an averaging operation over the single crystal (with volume V_g):

$$\boldsymbol{\varepsilon}_g^\mu = \langle \boldsymbol{\varepsilon}^\mu \rangle_g = \frac{1}{V_g}\int_\alpha \boldsymbol{\varepsilon}^\mu\, dV = \sum_\alpha f_\alpha \boldsymbol{\varepsilon}_\alpha^\mu \tag{12}$$

$$\mathbf{M}_g = \langle \mathbf{M} \rangle_g = \frac{1}{V_g}\int_\alpha \mathbf{M}\, dV = \sum_\alpha f_\alpha \overrightarrow{M_\alpha}. \tag{13}$$

The macroscopic magnetization is obtained through an averaging operation over the whole volume V of the polycrystal [17]:

$$\overline{\mathbf{M}} = \langle \mathbf{M} \rangle_V = \langle \mathbf{M}_g \rangle_V \tag{14}$$

The macroscopic magnetostriction strain is obtained through an averaging operation over the whole volume V of the polycrystal [17]:

$$\overline{\boldsymbol{\varepsilon}^\mu} = \langle {}^t\mathcal{B}_\sigma : \boldsymbol{\varepsilon}^\mu \rangle_V = \langle {}^t\mathcal{B}_\sigma : \boldsymbol{\varepsilon}_g^\mu \rangle_V \tag{15}$$

If the material exhibits a crystallographic texture, then this average operation is not made uniformly among all possible orientations g for the grains but in accordance with the orientation

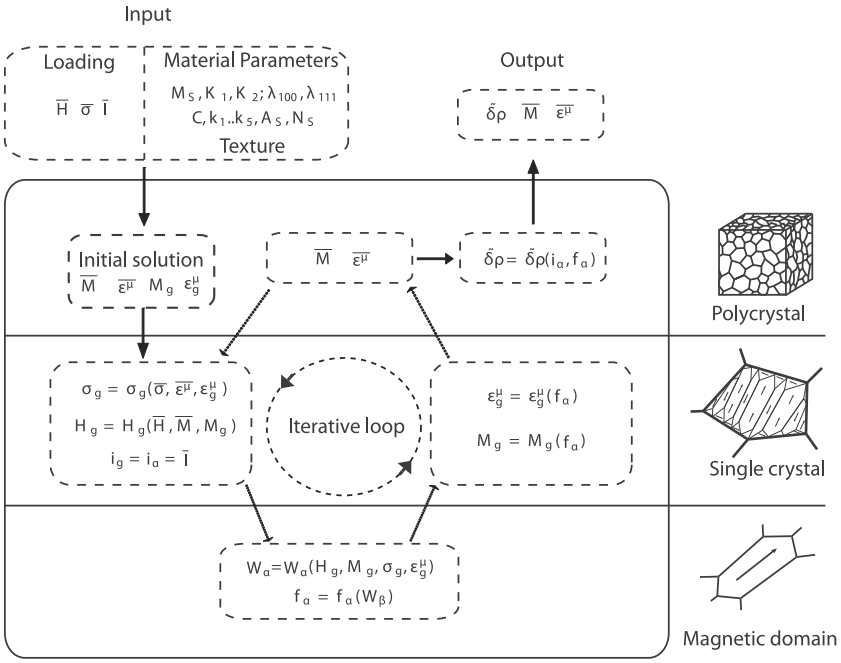

Fig. 4. Calculation algorithm.

distribution function of the polycrystal. This is why crystallographic texture effects are included in the proposed model.

Finally, the effective macroscopic conductivity $\tilde{\varsigma}$ ($\varsigma = 1/\rho$) is obtained through a self-consistent (Bruggeman) approach [19]:

$$\tilde{\varsigma} = \frac{\left\langle \frac{\varsigma_\alpha}{2\tilde{\varsigma} + \varsigma_\alpha} \right\rangle_V}{\left\langle \frac{1}{2\tilde{\varsigma} + \varsigma_\alpha} \right\rangle_V} \tag{16}$$

2.4. Calculation algorithm

The generic algorithm for the self-consistent calculation of the AMR response of thin films is given in Fig. 4.

The input data consists of the applied loading (magnetic field $\overline{\mathbf{H}}$, stress $\overline{\boldsymbol{\sigma}}$ and current $\overline{\mathbf{I}}$) and material parameters. Most of the material parameters are the classical single crystal constants except two adjustment parameters A_S and N_S. The parameter A_S can be readily identified from the initial slope of the anhysteretic magnetization curve [17], and N_S is related to the ratio between the grain size and the film dimensions [20]. The determination of the value of N_S is discussed in the last part of the paper. The crystallographic texture of the material is also needed under the form of an orientation distribution function, for example measured from Electron Back Scattering Diffraction (EBSD). The calculation being self-consistent, an initial starting point is needed for the macroscopic magnetization and magnetostriction strain. An initial guess is also needed for magnetization and magnetostriction at the grain scale. A uniform strain and magnetization hypothesis is usually chosen at this stage. It must be noticed that this initial choice does not affect the final solution but it has an impact on the convergence speed of the process.

From this data, the localization process is started to define the local loading ($\mathbf{H}_g$, $\boldsymbol{\sigma}_g$ and $\mathbf{i}_g$, Eqs. (1)–(3)). The free energy for each domain family is then computed (Eq. (5)), allowing us to define the volume fractions for each domain family (Eq. (11)). The material response is then computed at the grain scale (Eqs. (12) and (13)) and at the macroscopic scale (Eqs. (14) and (15)). The process is performed iteratively until the convergence on $\overline{\mathbf{M}}$ and $\overline{\boldsymbol{\varepsilon}^{\mu}}$ is reached. The macroscopic resistivity is then obtained with Eq. (16).

3. Application to permalloy thin films

In this part, we investigate the properties of a $Fe_{11}Ni_{89}$ polycrystal. This type of permalloy is often used in AMR sensors due to its significant AMR effect (# 2%).

3.1. Calculation parameters

The material constants of permalloy single crystal can be found in the literature. The parameters used in the present simulation are defined in Tables 1 and 2.[1]

The adjustment parameters A_S and N_S have been assigned the values of 0.032 m^3/J and 800 J/m^3, respectively.

In order to describe the possible orientation $\boldsymbol{\alpha}$ for the magnetization in the domain families, a set of 10,242 orientations optimally distributed on a unit sphere has been used for each crystallographic orientation [18].

The sharp crystallographic texture of AMR thin films resulting from the fabrication process is approximated by a perfect $\{hkl\}\langle 111\rangle$ texture. Each grain of the polycrystalline film is assumed to have $\langle 111\rangle$ direction aligned along the x direction. The plane normal to this $\langle 111\rangle$ direction is then obtained from uniformly distributed rotation around the $\langle 111\rangle$ direction. The corresponding pole figures are given in Fig. 5. A distribution of 180 grain orientations has been used. The use of a thin film with such a crystallographic texture makes the x direction an easy magnetization axis (due to the negative magnetocrystalline anisotropy constants, easy axis are $\langle 111\rangle$ directions for $Fe_{11}Ni_{89}$ single crystal).

3.2. Modeling results

As it is usually done in such devices, a bias magnetic field has been applied along the x direction. Due to the *barber-pole*

[1] Döring's constants are those of $Fe_{15}Ni_{85}$ but are assumed to be similar to those of $Fe_{11}Ni_{89}$.

Table 1
Physical constants used for the modeling (from measurement of single crystal properties [21,23]).

Coefficient	M_S	K_1, K_2	λ_{100}, λ_{111}	C_{11}, C_{12}, C_{44}
Unit	A/m	kJ/m^3	–	GPa
$Fe_{11}Ni_{89}$	7.50×10^5	-1, -2	-15, -10 ($\times$ 10^{-6})	243, 148, 122

Table 2
Constants for Döring expression (from measurement of single crystal properties [24]).

Coefficient	k_1	k_2	k_3	k_4	k_5
$Fe_{15}Ni_{85}$	0.0518	0.0478	−0.0243	−0.0139	0.0259

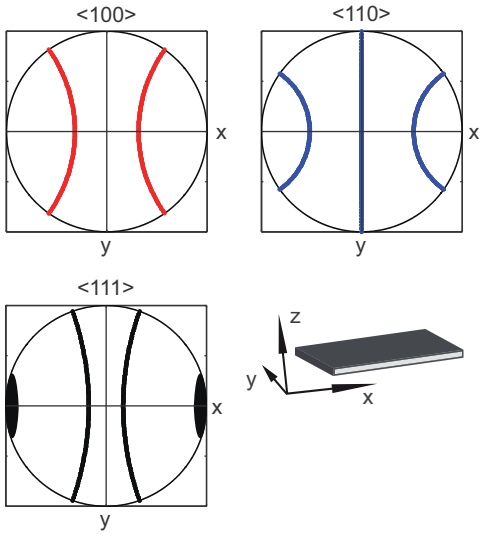

Fig. 5. ⟨100⟩, ⟨110⟩ and ⟨111⟩ pole figures for the AMR thin film (perfect {*hkl*} ⟨111⟩ fiber, 180 orientations).

configuration, the electric current is assumed to be oriented at 45° in the plane *xy* (see Fig. 3).

The change in resistivity as a function of the applied field in the measurement direction (*y*) is plotted in Fig. 6 for several bias fields (applied in the *x* direction). This result can be compared to measurements performed on a Philips commercial AMR sensor [25] (Fig. 7). The output voltage of the sensor is expected to be proportional to the change in resistivity (Fig. 6), the ratio depending on the specific electronic circuit used in the device.

Although the particular composition and crystallographic texture of the permalloy used in the Philips AMR sensor are unknown, a good qualitative agreement is obtained between modeling and measurement. The increase in resistivity is approximately linear with respect to the applied field up to a point corresponding to a configuration in which a large number of magnetic domains are parallel to the electric current (leading to the maximum resistivity). The resistivity then decreases while the magnetic domains tend to align along the direction of the applied magnetic field, closer and closer to the *y* direction. The initial linear stage of this curves defines the range of measurement of the sensor. High bias fields provide higher variations of resistivity and wider linear range but the slope – representative for the sensitivity of the sensor – is then lower. These effects are well captured by the model. The predicted level for the change in resistivity is much lower when no bias field is applied compared to the 1 kA/m bias field. This is not in accordance with the

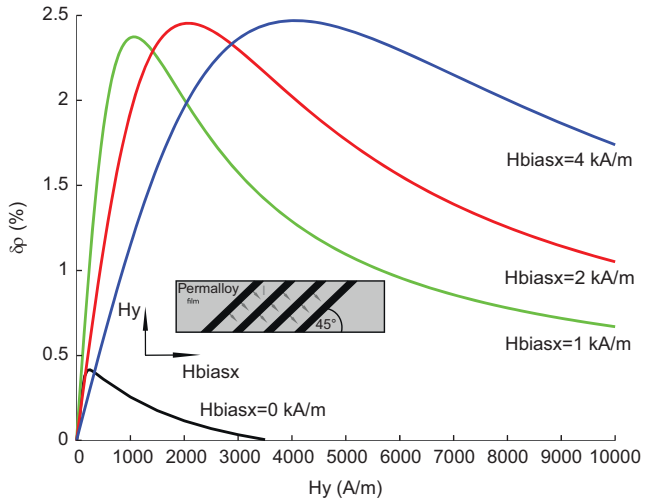

Fig. 6. Change in resistivity versus applied field for several bias field levels—modeling results.

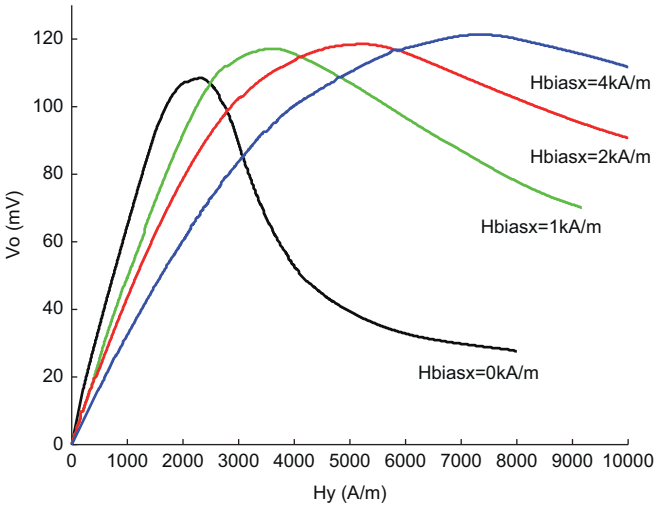

Fig. 7. Change in output voltage versus applied field for several bias field levels—experimental results from [25].

experimental observation. It probably means that the anisotropy of the thin film has been underestimated in the calculation. However as soon as a significant bias field is applied, it dominates the behavior of the sensor, and the model gets consistent with the experimental observation. The range of linearity of the AMR thin film is also underestimated by the model. The peak value of the curves is obtained for lower values of the applied magnetic field H_y. This is related to the fact that hysteresis effects have not been introduced in the modeling. The predicted curves are reversible whereas the resistivity versus total magnetic field experimental curves exhibit a hysteresis cycle – not shown in Fig. 7. The anhysteretic representation stands inside this hysteresis cycle. This discrepancy should not affect the accuracy of the prediction of the sensitivity of the sensor, but will only allow relative comparisons concerning the range of measurement.

4. Discussion

For the purpose of the discussion, we first define the sensitivity *S* and range of measurement H_{max} of an AMR sensor (see Fig. 8). The sensitivity *S* is defined as the slope of the linear part of

the curve. The range of measurement is the applied field value from which the resistivity change becomes non linear with the applied field. The loss of linearity is defined by a switch of δH with respect to the linear response (see Fig. 8). In the following, we will use the arbitrary value of $\delta H = 5$ A/m. The minimum detectable level of magnetic field is mainly related to the electronic circuit of the sensor and has not been considered in this work focused on the material AMR behavior.

4.1. Bias field effect

As seen in Fig. 6, the application of a bias field significantly increases the range of measurement of the sensor. This effect is illustrated in Fig. 9. But the main role of the bias field (along the direction x) is to ensure that the sensor is unidirectional, meaning that it is sensitive only in direction y of the film. This effect can be captured by the model. Fig. 9 shows the sensitivity of the permalloy thin film sensor in directions x and y as a function of the bias field $Hbias_x$. The sensitivity in direction z has not been plotted. Due to the surface effect – resulting from the thin film geometry – the material is very hard to magnetise in direction z, the sensitivity in that direction is then very low, almost zero.

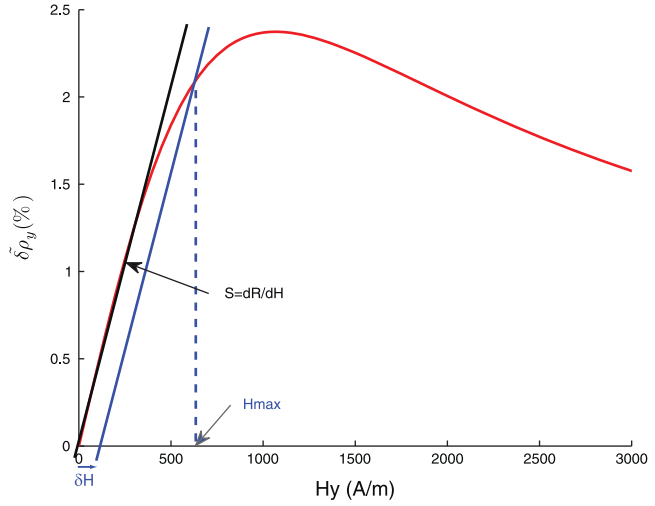

Fig. 8. Definition of the sensitivity S and the range of measurement H_{max} on a magnetoresistive curve.

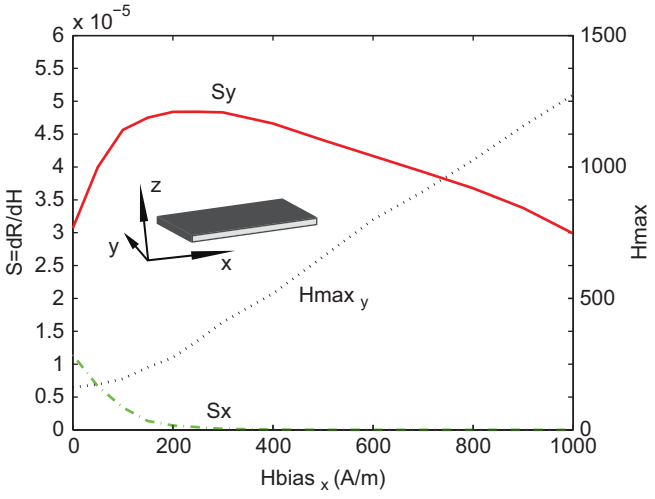

Fig. 9. S_x, S_y and $H_{max\,y}$ as a function of the bias field applied in the x direction.

As soon as the bias field level reaches a yield value (approximately 250 A/m in that case, in accordance with standard bias field levels in AMR sensors), the sensitivity along direction x vanishes. This is due to the saturation of the material with a magnetization along direction x. On the other hand, the sensitivity in the direction y first increases with the bias field and then decreases, so that an optimal value for the bias field can be obtained. In the case illustrated in Fig. 9, a minimum bias field of 250 A/m is required but the intensity of the bias field can be adjusted depending on the desired compromise between sensitivity and range of measurement. The proposed model is then a tool to optimize this choice.

4.2. Influence of the film thickness

The influence of the film thickness w can also be investigated through the variation of the parameter N_S. For a given grain size of the material, N_S is inversely proportional to the film thickness [20]. In the case of the sensor configuration studied above with a strong in plane ⟨111⟩ fiber and an in-plane magnetic field, the role of the thickness is weak since the magnetization spontaneously remains in-plane. On the other hand, if the magnetic field is normal to the thin film plane, then the thickness plays a significant role. To study this role, we focus now on a slightly different AMR sensor.

The influence of the film thickness on the sensing properties of *single-path* AMR sensors has been studied experimentally by Tumanski [6]. The structure of this type of sensors has been previously presented in this paper (Fig. 2). The main difference from the *barber-pole* sensors is the direction of the current as it aligns here in the direction of the macroscopic easy axis, x, in the film plane. The magnetic field is applied perpendicular to the film plane (z direction). Fig. 10 shows the modeling results compared to the experimental observations. The parameter N_S has been fitted using the experimental curve with 50 μm thickness as a reference and the same model parameters as before. Assuming that N_S is inversely proportional to the film thickness, its values can be determined from this first fitting in order to predict the curves with 25 and 75 μm thicknesses. The comparison between numerical and experimental results gives satisfying results. The model can predict the influence of the film thickness on the sensing properties.

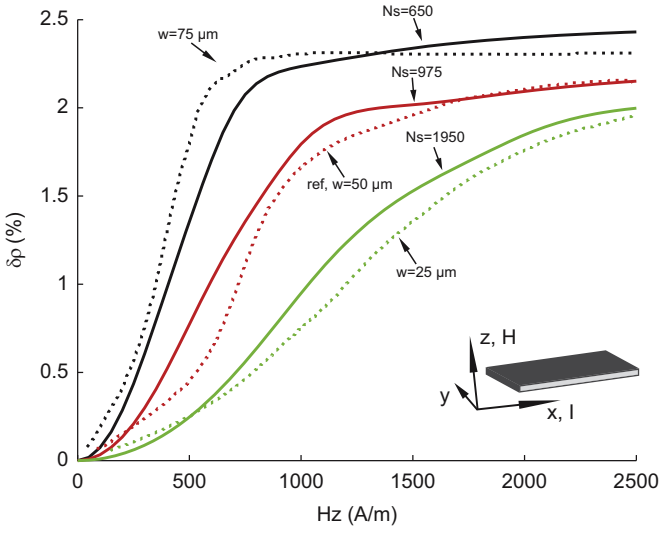

Fig. 10. Change in resistivity versus applied field for several film thicknesses—modeling (lines) and experimental results [6] (dotted lines).

5. Conclusion

A numerical tool for the behavior of AMR thin film sensors has been proposed. It is based on a magneto-elastic multiscale model combined with a local model for material resistivity (Döring model). This approach accounts for the specific features of AMR sensors (thin film structure, *barber-pole* configuration or sharp crystallographic texture). It could also be extended to amorphous or nanocrystalline alloys by introducing appropriate anisotropy terms. The model has been applied to the modeling of a polycrystalline permalloy thin film sensor. This numerical tool allows us to investigate the nonlinear magnetoresistive behavior of this type of structures in 3D. It can be used for optimization purpose to define optimal material composition, crystallographic texture, film thickness or bias field level for specific applications.

References

[1] S. Chikazumi, Introduction to Ferromagnetic Materials, Addison-Wesley, 1997.
[2] D.J. Adelerhof, W. Geven, New position detectors based on AMR sensors, Sensors and Actuators A 85 (2000) 48.
[3] Honeywell SSEC, Linear/Angular/Rotary Displacement Sensors, Technical Report HMC1501-1512, 〈www.ssec.honeywell.com〉.
[4] J. Vcelák, P. Ripka, J. Kubík, A. Platil, P. Kaspar, AMR navigation systems and methods of their calibration, Sensors and Actuators A 123–124 (2005) 122.
[5] P. Mlejnek, M. Vopálenský, P. Ripka, AMR current measurement device, Sensors and Actuators A 141 (2008) 649.
[6] S. Tumanski, Thin Film Magnetoresistive Sensors, IOP Publishing, 2001.
[7] J. Kubik, J. Vcelak, P. Ripka, On cross-axis effect of the anisotropic magnetoresistive sensors, Sensors and Actuators A 129 (1–2) (2006) 15.
[8] N.A. Stutzke, S.E. Russek, D.P. Pappas, M. Tondra, Low-frequency noise measurements on commercial magnetoresistive magnetic field sensors, Journal of Applied Physics 97 (10) (2005) 10Q107.
[9] E. Zimmermann, A. Verweerd, W. Glaas, A. Tillmann, A. Kemna, An AMR sensor-based measurement system for magnetoelectrical resistivity tomography, IEEE Sensors Journal 5 (2) (2005) 233.
[10] T.R. McGuire, R.I. Potter, Anisotropic magnetoresistance in ferromagnetic 3d alloys, IEEE Transactions on Magnetics 11 (1975) 1018.
[11] J. Li, S.L. Li, Z.W. Wu, S. Li, H.F. Chu, J. Wang, Y. Zhang, H.Y. Tian, D.N. Zheng, A phenomenological approach to the anisotropic magnetoresistance and planar Hall effect in tetragonal $La_{2/3}Ca_{1/3}MnO_3$ thin films, Journal of Physics: Condensed Matter 22 (2010) 146006.
[12] M.J. Haji-Sheikh, Accurate Model of Saturated AMR Wheatstone Bridge Sensor Against a 48 Pole Pair Ring-Magnet, in: First International Conference on Sensing Technology, 2005.
[13] H. Beltran, C. Reig, V. Fuster, D. Ramírez, M.D. Cubells-Beltrán, Modeling of magnetoresistive-based electrical current sensors: a technological approach, IEEE Sensors Journal 7 (2007) 1532.
[14] K. Leitis, T. Halim, Modeling of a 3D magnetic field (AMR) sensor, in: IEEE International Conference on Microwaves, Communications, Antennas and Electronics Systems (COMCAS), 2011.
[15] T.R. Koehler, B. Yang, W. Chen, D.R. Fredkin, Simulation of magnetoresistive response in a small Permalloy strip, Journal of Applied Physics 73 (10) (1993) 6504.
[16] K. Shiiki, Y. Mitsui, Y. Hirata, Effect of anisotropy dispersion on magnetization process in magnetoresistive sensor films, Journal of Applied Physics 79 (5) (1996) 2590.
[17] L. Daniel, O. Hubert, N. Buiron, R. Billardon, Reversible magneto-elastic behavior: a multiscale approach, Journal of the Mechanics and Physics of Solids 56 (2008) 1018.
[18] L. Daniel, N. Galopin, A constitutive law for magnetostrictive materials and its application to Terfenol-D single and polycrystals, European Physical Journal—Applied Physics 42 (2008) 153.
[19] A. Bartók, L. Daniel, A. Razek, Micro-macro modelling of stress-dependent anisotropic magnetoresistance, Journal of Physics D: Applied Physics 44 (13) (2011) 135001.
[20] O. Hubert, L. Daniel, Multiscale modeling of the magneto-mechanical behavior of grain-oriented silicon steels, Journal of Magnetism and Magnetic Materials 320 (7) (2008) 1412.
[21] R.M. Bozorth, Ferromagnetism, Van Nostrand, 1951.
[22] N. Buiron, L. Hirsinger, R. Billardon, A multiscale model for magneto-elastic couplings, Journal de Physique IV 9 (1999) 139.
[23] A. Kanrar, U.S. Ghosh, The variation of elastic constants of nickel-iron single crystal alloys from 78.76 to 300 K, Journal of Physics and Chemistry of Solids 44 (1983) 457.
[24] L. Berger, S.A. Friedberg, Magnetoresistance of a permalloy single crystal and effect of 3d orbital degeneracies, Physical Review 165 (1968) 670.
[25] Application Note, General Magnetoresistive Sensors for Magnetic Field Measurement, Technical Report KMZ10, Philips Semiconductors, 〈http://www.philips.com〉, 2000.